Time resolved ultraviolet absorption spectroscopy of pulsed fluorocarbon plasmas

Brett A. Cruden,[a] Karen K. Gleason, and Herbert H. Sawin
Department of Chemical Engineering, Massachusetts Institute of Technology, Cambridge, Massachusetts 02139-4307

(Received 25 February 2000; accepted for publication 30 October 2000)

Ultraviolet absorption spectroscopy has been used to quantitatively measure CF_2 transients in 1 Torr capacitively coupled pulsed plasmas. Time resolved concentrations were obtained for both tetrafluoroethylene (TFE) and hexafluoropropylene oxide (HFPO) feed gases. In the TFE plasma, the CF_2 production kinetics follow a first order rise to concentrations of $\sim 10^{14}/cm^3$. In the plasma afterglow, a net production of CF_2 is observed for a few milliseconds before the transient becomes dominated by a second order recombination process. In the HFPO plasma, three distinct regimes are observed in the plasma on time. Two production regimes exist, one presumably due to HFPO dissociation and the second due to an unknown source, beginning about 5 ms into the on time. Finally, the CF_2 concentration passes through a maximum and decreases to steady state. The afterglow processes are similar to those observed for TFE. The production observed in the off time is believed to be related to surface processes.
[DOI: 10.1063/1.1334936]

I. INTRODUCTION

The study of fluorocarbon plasmas is of great interest for their applications in silicon dioxide etching.[1,2] Recently, attention has been paid to using fluorocarbon plasmas to produce low dielectric constant fluorocarbon thin films.[3] However, details of fluorocarbon surface and gas phase chemistry are still not fully understood, and much research is still ongoing in this area.[1,2,4] For film deposition, the use of pulsed plasmas has shown the capability to control film chemistry and composition.[5] Pulsing of the plasma can control film composition in several ways. First, pulsing reduces plasma surface interactions, which include ion bombardment and ultraviolet (UV) irradiation effects. During the plasma off time, long-lived radicals (such as CF_2) will still interact with the surface after the ion flux has decayed, thus altering the effective neutral to ion ratios. Additionally, pulsing of the plasma brings the gas phase composition out of steady state. Temperature and concentration transients will exist that are not present in a continuous plasma. The degree of fragmentation of precursors and intermediates will be reduced because of less exposure time to the plasma. Other properties, such as plasma densities and temperatures, will also be affected by pulsing. In order to understand mechanistically how pulsing gives control of film properties, it is desirable to understand how pulsing affects the gas phase chemistry.

The technique of UV absorption spectroscopy has been used extensively for diamond like carbon deposition and other deposition and etching environments.[6] The use of UV absorption spectroscopy for detection of CF_2 is a relatively simple technique, however it has only seen a few applications.[7–9] More commonly, CF_2 concentrations have been measured by infrared absorption techniques[10–12] and laser induced fluorescence.[13–16] Time resolved measurements of CF_2 concentrations in pulsed plasmas have been made on relatively short (<10 ms) time scales, primarily in plasmas relevant to etching conditions.[10,14,17] Other researchers have measured CF_2 loss for longer pulse times (~10–100 ms) at lower pressures (50–400 mTorr), and have observed first order loss and creation mechanisms.[11,16] Quantitative transients have been recorded in the off time of a low pressure (~10 mTorr) C_4F_8 plasma,[18] with an initial off time production of CF_2, followed by a decay described by second order kinetics.

In this work, we look at the general behavior of CF_2 in depositing plasmas of tetrafluoroethylene (TFE) and hexafluoropropylene oxide (HFPO). Both precursors are expected to readily form CF_2 upon electron impact:[19,20]

$$CF_2{=}CF_2 \xrightarrow{e^-} 2CF_2, \tag{1}$$

$$CF_3-\underset{\underset{O}{\vee}}{CF}-CF_2 \xrightarrow{e^-} CF_3-\underset{\underset{O}{\|}}{CF}+CF_2. \tag{2}$$

The presence of oxygen in HFPO, however, will add an etching component to the HFPO plasma chemistry.

II. EXPERIMENT

A diagram of the experimental setup is shown in Figure 1. The deposition is performed in a homebuilt parallel plate reactor. The precursor gas flows through a showerhead in the top electrode, at a pressure of 1 Torr and a flow rate of 50 sccm. The TFE precursor is passed through a silica gel scrubber to remove a limonene inhibitor before it is fed to the chamber. Typically, an on time peak power of 100 W is used to strike the plasma. The substrate sits on the bottom electrode, which is powered by a pulse generator/function

[a]Electronic mail: bcruden@alum.mit.edu

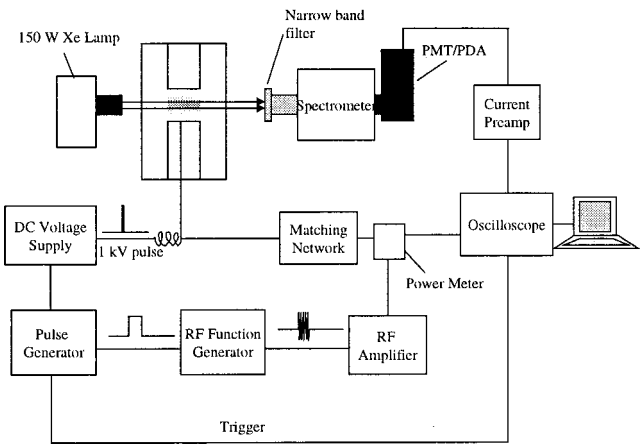

FIG. 1. Diagram of the experimental setup. A pulsed plasma is produced in the reactor, and a photomultiplier tube is used to measure absorption as a function of time.

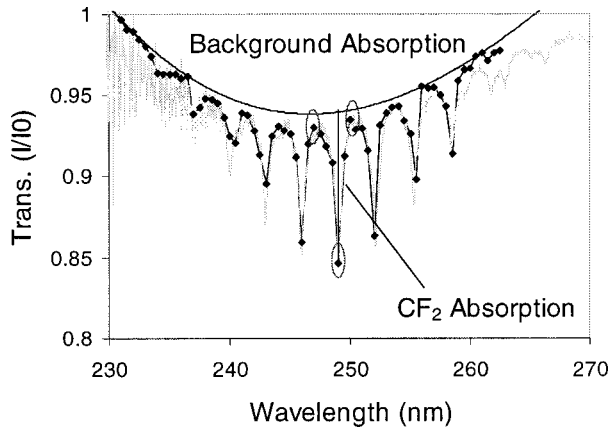

FIG. 2. Sample absorption spectrum from a continuous TFE plasma taken with the PDA. The continuous curve represents data obtained here, while the points are a fit based on the cross sections of Sharpe *et al.* (see Ref. 21). The three circled data points are the points used for the time resolved measurements.

generator/rf amplifier train. The substrate temperature is maintained at either 20 °C by circulating water or at 50 °C with circulating oil. The chamber wall temperature can also be controlled from room temperature (~28 °C) to 150 °C by heating tape. In depositing pulsed plasmas with long off times (>10 ms), it is not uncommon to have difficulties in achieving a reproducible plasma breakdown. To assist with this problem, a 1 kV dc pulse is applied at the beginning of each pulse period. The voltage transients from this pulse are gone within the first 2 ms, and the pulse does not appear to greatly affect deposition behavior or the plasma chemistry measured here. For the experiments discussed here, a pulse duty cycle of 100 ms on/400 ms off is used, so that the plasma has sufficient on and off periods to approach steady state.

For the UV absorption measurements, a 150 W Xe lamp with collimated optics projects light through the plasma from one viewport, and is collected by a 27 cm spectrograph with an UV enhanced 1200 g/mm grating at the opposite side of the chamber. A band pass filter [250 nm peak, 60 nm full width at half maximum (FWHM)] is used to remove stray light and higher order diffraction. Data are collected by either a photodiode array (PDA) or a photomultiplier tube (PMT). The PDA (Tracor Northern, TN-6112) is useful for obtaining spectra at several different wavelengths simultaneously. However, it cannot give millisecond scale time resolution and is only used to get a time-averaged signal. The PMT (Hammamatsu, R955) is only able to read one wavelength at a time, but can give signals on the desired time scale. Signal to noise is improved by averaging the PMT signal over 500–5000 pulses via a LeCroy 9414 digital oscilloscope.

III. RESULTS AND DISCUSSION

As described previously,[9] the absorption intensity is determined by performing four scans, one with the lamp alone, one with the lamp and plasma, one with the plasma alone, and a background scan. The transmittance can then be found as follows:

$$Tr = \frac{I}{I_0} = \frac{I_{\text{plasma+lamp}} - I_{\text{plasma}}}{I_{\text{lamp}} - I_{\text{dark}}}. \tag{3}$$

This can then be related to the CF_2 density by the Beer–Lambert law:

$$\ln\left(\frac{I}{I_0}\right) = -\sigma L_{\text{eff}} n_{CF_2}. \tag{4}$$

The cross sections σ have been characterized by Sharpe *et al.*[21] The effective length, L_{eff}, depends on the radial profile of CF_2, described in the Appendix, where it is estimated at 26.2 cm.

Figure 2 shows a sample absorption spectrum from a continuous TFE plasma near 250 nm. The peaks apparent here are characteristic of the CF_2 absorption, and represent the $\tilde{A}^1B_1 \leftarrow \tilde{X}^1A_1$ transition.[21] However, to adequately fit this absorption spectrum, an additional absorption background must be introduced. The source of this background is unknown, although Booth *et al.* examined several possibilities for its source,[9] without reaching a satisfactory explanation. Its close coincidence with the CF_2 bands would suggest higher underlying vibrational or rotational states. However, the transition from the next vibrationally excited ground state (0,1,0) has maximum Franck–Condon factors at 263 nm.[22] Absorption due to this transition is observed in Fig. 2, but is far weaker than the rest of the background spectrum. The possibility of adsorption from rotationally excited states was explored by Booth *et al.*, but they were not able to fit this background absorption.[9] This leaves another species as the only possible explanation for this absorption. d'Agostino *et al.* have observed a continuum emission with similar properties to this absorption, and claim that this emission scales with F_2 concentration.[19] However, F_2 absorption observed in this wavelength region is weak and does not match this continuum.[23] It is still possible that this absorption is due to the same transition producing that continuum, if the continuum is due to something other than F_2.

To separate out this background signal from the CF_2 absorption in the time resolved measurements, absorption is

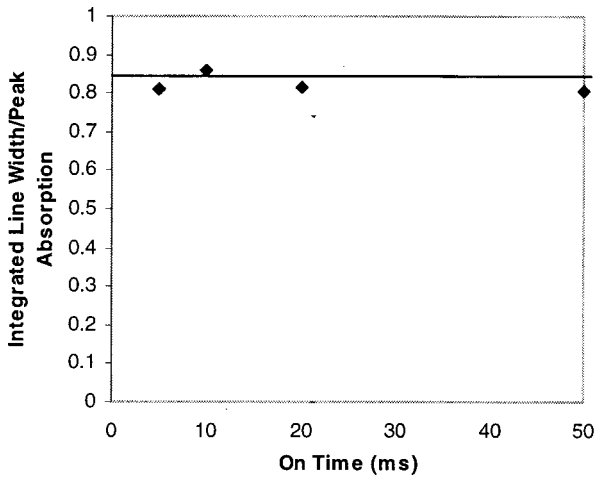

FIG. 3. Ratio of peak absorption (measured at 249 nm) to integrated line density (from 247 to 250 nm) after background subtraction. The data points are obtained from time averaged emission of TFE pulsed plasmas with an off time of 200 ms and varying on time. Shown for comparison, as the solid line, is the ratio for a continuous TFE plasma. The data shown here give a standard deviation from the mean value of about 5%.

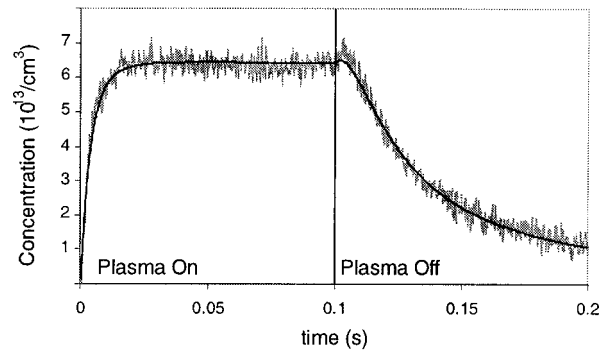

FIG. 4. Concentration of CF_2 as a function of time for a TFE plasma pulsed on for 100 ms and off for 400 ms. The substrate temperature is 20 °C and the chamber walls are 60 °C. The line through the data represents the fit of a simplified kinetic model.

measured at three different wavelengths (247, 249, and 250 nm), as indicated by the circles in Fig. 2. The absorption due to CF_2 and the background signal can then be separated out, assuming the background absorption cross section varies approximately linearly with wavelength between 247 and 250 nm:

$$\langle CF_2\rangle \approx -\frac{\ln(Tr_{249})-\frac{1}{3}[\ln(Tr_{247})+2\ln(Tr_{250})]}{L_{\mathrm{eff}}[\sigma_{249}-(\sigma_{247}+2\sigma_{250}/3)]}, \quad (5)$$

$$\langle \mathrm{Bkgd}\rangle \sim \sigma_{249}\langle CF_2\rangle - \frac{-\ln(Tr_{249})}{L_{\mathrm{eff}}}, \quad (6)$$

where σ_λ and Tr_λ are the CF_2 absorption cross section and overall transmittance at wavelength λ. $\langle CF_2\rangle$ represents the spatially averaged CF_2 density, while $\langle \mathrm{Bkgd}\rangle$ is the average density of species responsible for the background absorption. Since the cross sections for the background species are unknown (as are the species themselves), only a relative measurement can be made and its value will take on arbitrary units.

Measuring absorption at a single wavelength can produce errors in measurements if significant line broadening is observed. This line broadening can be due to factors such as optical thickness or changing rotational temperatures. To verify this approximation, the ratio of peak absorption intensity at 249 nm to integrated absorption intensity between 247 and 250 nm has been examined as pulse on time is varied in Fig. 3. Based on the standard deviation of these data, line broadening accounts for no more than a 5% error in the measurements. This is less than the estimated error in literature absorption cross sections of 15%–30%.[9,21]

There is also the possibility of deviation from the Beer–Lambert law at high species concentrations. [Note that these deviations from Beer–Lambert law should not be attributed to the overall absorption, but rather to the species concentration, i.e., Eq. (4) will hold even if the path length is varied.] The published cross sections were determined with CF_2 densities higher than $6\times10^{14}\,\mathrm{cm}^{-3}$, and still agreed well with the known kinetic behavior of CF_2 when the Beer–Lambert law was applied.[21] The concentrations observed in this work are somewhat less than that, so they should be consistent with the Beer–Lambert law.

Figure 4 shows the time varying profile of the CF_2 concentration for a TFE plasma pulsed on for 100 ms and off for 400 ms. During the on time, the CF_2 concentration rises from zero towards a steady state concentration of $6.4\times10^{13}/\mathrm{cm}^3$. For a 1 Torr total plasma pressure, this shows that the CF_2 concentration is less than 1% of the total concentration. The initial on time rise represents the formation of CF_2 by electron impact on the TFE precursor. Other sources for CF_2 formation are possible as on time increases, but are not distinguishable from the initial production trend. Steady state is reached when the combined rates of all CF_2 loss mechanisms equal the rate of CF_2 creation. Loss of CF_2 proceeds through both gas phase and surface based recombination pathways as well as through further electron impact dissociation.

On plasma extinction, electron impact processes can be expected to cease on a time scale much shorter than a millisecond[24] (based on the decay in optical emission from the plasma) and CF_2 will be depleted by recombination with itself, the wall, and other species. On longer time scales, CF_2 will be convectively removed from the chamber. Surprisingly, Fig. 4 reveals that when the plasma is shut off, the observed CF_2 concentration rises for the first 4–5 ms, and then decays back towards zero. For there to be production of CF_2 in the afterglow, there must be a production mechanism that does not require an electron impact process. At the end of the plasma on time, there are at least two production processes (one involving electron impact, and one not involving electron impact), and two consumption processes (electron impact dissociation and recombination), which together are at steady state. Once the plasma is turned off, the remaining production process proceeds at a faster rate than recombination. A simple kinetic model is used to explain this transient:

$$\mathrm{TFE}+e^-\rightarrow 2CF_2+e^-, \quad (1)$$

$$CF_2+e^-\rightarrow \text{other species}, \quad (7)$$

$$\text{plasma}\rightarrow I, \quad (8)$$

$$CF_2 + CF_2 \rightarrow TFE, \tag{9}$$

$$I \rightarrow CF_2, \tag{10}$$

where I is some unknown intermediate source. Equations (1), (7), and (8) are plasma activated processes, and thus occur only during the plasma on time. To fit the profiles shown here, the electron density and energy distribution are assumed to be constant, and their values are lumped into the rate coefficient, i.e.,

$$k_i = \int_{E_{th}}^{\infty} \sigma_i(E) f_e(E) \left(\frac{2E}{m_e}\right)^{1/2} dE, \tag{11}$$

where σ_i is the cross section for reaction i ($i=1$ or 7), m_e is the electron mass, and f_e is the electron energy distribution function.

The intermediate source is assumed to be created at a nearly constant rate by the plasma. If this is the case, transients in $[I]$ will be first order, with its time constant given by k_{10}. First order loss processes for CF_2 in the off time are assumed to be due solely to pumping, and not due to surface loss because the surfaces exposed to the plasma will be coated with a fluorocarbon film. In these types of plasmas, the surface loss rates are greatly reduced,[11,25] and decay is observed to occur primarily by a second order mechanism.[18] In the absence of ion bombardment, the sticking coefficient of CF_2 on a fluorocarbon surface has been measured to be on the order of 10^{-5} or less.[26] The conditions in the plasma afterglow for this work are expected to be similar to these. In spite of this evidence, it is still possible that first order surface losses are not negligible, and that will affect the results of this model. It is possible to obtain an adequate fit to the data by using a somewhat higher first order loss process. However, it is not possible to fit the data with a combination of literature values of k_9 and an adjustable first order loss coefficient. Thus, the first order loss is held constant here, and the second order loss is adjusted.

Considering these reactions, the following mole balances are derived:

on time:

$$\frac{d[CF_2]}{dt} = 2k_1[TFE] + k_{10}[I] - (1/\tau + k_7)[CF_2] - 2k_9[CF_2]^2,$$

$$\frac{d[TFE]}{dt} = \frac{Q_{TFE}}{V} - (1/\tau + k_1)[TFE] + k_9[CF_2]^2, \tag{12}$$

$$[I] = [I]_0(1 - e^{-k_{10}t}),$$

off time:

$$\frac{d[CF_2]}{dt} = k_{10}[I] - \frac{[CF_2]}{\tau} - 2k_9[CF_2]^2,$$

$$[I] = [I]_0 e^{-k_{10}t}, \tag{13}$$

where τ is the residence time in the plasma, and is calculated by the following equation:

$$\tau = \frac{V}{Q_{TFE}}\left(\frac{760}{P\,(\text{Torr})}\right); \tag{14}$$

TABLE I. Fit parameters for a simplified TFE model for different wall and substrate temperatures.

Fit parameter (units)	$T_{wall}=30$ °C $T_{sub}=20$ °C	$T_{wall}=60$ °C $T_{sub}=20$ °C	$T_{wall}=150$ °C $T_{sub}=20$ °C	$T_{wall}=150$ °C $T_{sub}=50$ °C
k_1 (s^{-1})	0.217	0.250	0.207	0.207
k_7 (s^{-1})	294	256	152	178
k_{10} (s^{-1})	122	119	133	198
k_9 ($cm^3\,s^{-1}$)	3.19×10^{-13}	3.45×10^{-13}	1.68×10^{-13}	1.37×10^{-13}
I_0 (cm^{-3})	7.52×10^{12}	3.28×10^{13}	4.07×10^{13}	4.51×10^{13}

V is the volume of the plasma ($\approx$158 cm^3), and Q_{TFE} is the flow rate of TFE (50 sccm). Note that this residence time must be consistent with the control volume used in the mole balance, Eqs. (12). Because the chamber is not believed to be well mixed (based on the calculated Peclet number in the Appendix), these calculations will give the average concentration within the plasma volume. This will introduce some error in that this experimental technique gives the average concentration across the path of the UV beam. Using the value of L_{eff} given in the Appendix should give some correction to this error.

In making this calculation, it is assumed that the molar content of the gas inlet does not change greatly in the plasma. In reality, deposition and formation of larger molecular weight fragments will increase the residence time, since the chamber is held at constant pressure, rather than at a constant volumetric flow rate. Deposition rates during the on time are approximately 1 μm/min, which corresponds to a molar consumption of ~10% of the feed gas. At the same time, formation of lower molecular weight fragments and elevated neutral temperatures will decrease the residence time. It is probably safe to assume that the control valve cannot respond on a time scale to alter the flow rate over the course of a single pulse.

The value of k_9 is determined by fitting the off time decay 5 ms into the off time, after the maximum concentration has been reached. Values for I_0 and k_{10} are then obtained by Euler integrating equations (13) over the entire off time and performing nonlinear regression. Equations (12) are then Euler integrated and nonlinear regression is performed on k_1 and k_7. For a self-consistent model, the initial conditions must be varied until they are equal to the values at the end of the off time. The parameters are then adjusted simultaneously and minimized by the conjugate gradient method. The fit parameters obtained here, for different temperature conditions, are shown in Table I.

It has been observed previously that an increased wall temperature results in a higher CF_2 concentration in the gas phase, and this dependence is commonly attributed to a reduction in surface loss processes.[27] The wall and wafer temperatures are also observed to play a significant role in the fit parameters obtained here. The CF_2 creation rate attributed to electron impact on TFE, or k_1, shows a variation of ~20%. This variation is small enough to be due to variations in plasma matching conditions. The first order loss process for CF_2, however, shows a fairly significant dependence on wall temperature, dropping significantly as the wall temperature is

increased to 150 °C. As wall temperature should not affect electron impact processes, this would suggest that, at lower temperatures where a fluorocarbon film is formed, CF_2 can be lost to the surface during the plasma on time. This change in first order loss rate is not seen in the plasma off time, indicating this loss process is dependent on ion bombardment. This sort of enhancement of CF_2 sticking probability with ion bombardment has been experimentally shown.[28]

The fit parameters obtained for k_9 at wall temperatures of 150 °C are slightly higher than those observed in the literature for two-body gas phase recombination of CF_2. Based on literature values, we can calculate a self-recombination rate between 3.78×10^{-14} and $7.19\times10^{-14}\,\mathrm{cm^3/s}$ at 150 °C.[29] At lower wall temperatures, the observed recombination coefficient increases by about 2.5 times, whereas the literature recombination coefficients should decrease at lower temperatures. This trend suggests that there is a recombination process involving the chamber walls. Second order surface aided recombination has not previously been observed for CF_2, however it has been suggested as a mechanism for fluorine depletion.[30] This dependence may not have been observed in other systems because of the nature of the wall surface. In this work, the wall and wafer will be coated with a relatively thick (several microns) fluorocarbon film at temperatures below 150 °C. Two possible interpretations for the mechanism here are given. One possibility is that a single CF_2 molecule is recombining with an activated surface site. This could give an apparent second order behavior because the surface site density will decrease at the same rate as the CF_2 density. The second possibility is that the surface is aiding CF_2 self-recombination by either physisorbing CF_2 species or entrapping them within pores in the film. In either case, the temperature trends seen here suggest that the observed recombination rate will approach the literature values if the wafer temperature is increased to 150 °C.

Other more subtle effects may be possible, including an altered effective path length from Eq. (4), changing residence time, or formation/recombination of other species on the wall. Other time resolved measurements of CF_2 have observed first order loss mechanisms due to recombination with other gas phase neutrals and surfaces in CF_4 (Refs. 11 and 17) and a second order loss mechanism in C_4F_8.[18] This suggests that F-rich plasmas, such as CF_4, produce species (or surfaces) that combine more readily with CF_2. TFE would be expected to be more akin to its dimer, C_4F_8. It should be noted that a first order loss mechanism is not sufficient to fit the decay observed in this work.

There are many possible explanations for the CF_2 producing intermediate, *I*. However, considering several independent measurements of surface production of CF_2,[10,11,13,15,31] even in the afterglow,[14,18] it seems likely this production is a surface production process. The fact that increasing surface temperatures increase this production (as witnessed by the dependence of I_0 on temperature) supports this assertion. The values of I_0 obtained here correspond to no more than 0.14 monolayer if we consider the source to be on the electrode surfaces and reactor walls. The data here show that this surface production mechanism could also be a cause of the observed dependence of CF_2 concentration on wall temperature.[27]

This apparent CF_2 flux observed from the surface has been attributed to several mechanisms. Haverlag's suggestion of production from dissociative collisions in the sheath has been invalidated by Booth *et al.*, who have attributed the production mechanism to dissociation of ions on the surface.[13] However, under polymerizing conditions, the rate of CF_x production exceeds the ion flux measurements.[11,14] In our system, the CF_2 production decays with a characteristic lifetime ($1/k_{10}$) of 5–8 ms, while the ions should be nearly extinguished in less than 1 ms.[14] Capps *et al.* have suggested some other chemical mechanisms involving CF_3 or CF interactions with the surface.[31] Off time transients of CF consistent with this hypothesis have been observed, but not under all conditions.[18] Other studies have seen a net creation, rather than consumption, of CF (Refs. 11 and 14) and CF_3 (Ref. 11) at the surface.

Cunge and Booth have suggested that this process may be due to the diffusion of CF_2 out of the polymer surface.[14] With this hypothesis, one could estimate the solid diffusivity of CF_2 based on the one-dimensional diffusion equation:

$$\frac{\partial[\mathrm{CF_2}]}{\partial t}=D\frac{\partial^2[\mathrm{CF_2}]}{\partial z^2}, \tag{15}$$

$$k_{10}=\frac{1}{\tau_D}\sim\frac{D}{l^2}. \tag{16}$$

Based on the fit value for k_{10} and an estimated mixing length, *l*, of 30 Å, we get a diffusivity $D\sim1.1\times10^{-11}$–$1.8\times10^{-11}\,\mathrm{cm^2/s}$. This number is a couple of orders of magnitude lower than typical solid diffusivities. If we assume the CF_2 is escaping from the bulk, and not the surface, of the film, a more realistic diffusivity can be found, assuming the film is sufficiently thick. Other possibilities include the creation of CF_2 on the surface from higher molecular weight species, in which case the production will be controlled by the lifetime of these species in the plasma afterglow. Also, the film, as deposited, may undergo some internal reactions to produce CF_2. The dependence of k_{10} on the wafer temperature is consistent with that of the deposition rate, which shows a negative activation energy of 11.2 eV.[32] This at least suggests that CF_2 surface production is closely linked to the film growth rate. The dependence of I_0 on the wafer and wall temperature also suggests that the production may be due to film rearrangement.

The variation in background signal at 249 nm [Eq. (6)] as a function of time is shown in Fig. 5. The signal has a somewhat different variation than the CF_2. There are two apparent transients in both the on and off signals. The slower rise and fall are consistent with a transient controlled by flow out of the reactor. One can only speculate as to the source of the faster transient, be it a recombination with the surface or other gas phase species.

The transient for a 100/400 HFPO plasma is shown in Fig. 6. This variation is considerably more complex than that of TFE. The on time can be divided into three regimes. The first involves an initial production of CF_2 and its approach to a local maximum. It makes sense to attribute this initial pro-

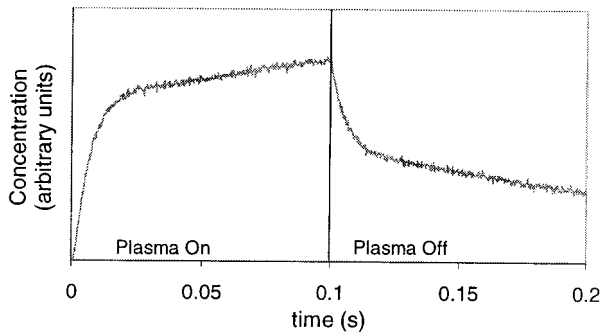

FIG. 5. Variation of the background signal for a TFE 100/400 plasma. This absorption transient differs from that of CF_2, suggesting the absorption source is something other than rotationally excited states.

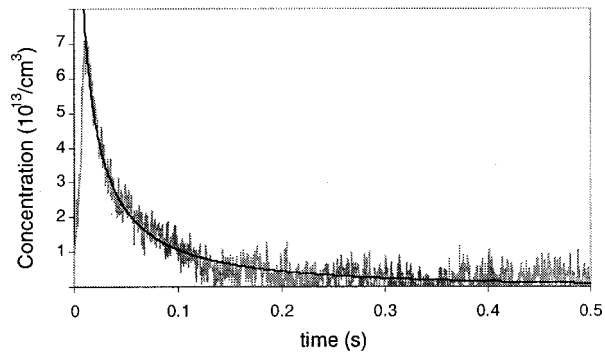

FIG. 7. Transient for HFPO plasma 10 ms on/490 ms off. The line fit is for a second order decay mechanism. This trend is not well fit by a first order decay.

duction to dissociation of the feedstock gas, reaction (2). After about 5 ms, a secondary production mechanism begins. It is not obvious what the source of this secondary production mechanism might be. The CF_2 concentration goes through a maximum at about 20 ms, and then falls down towards steady state. In the off time, an initial production followed by CF_2 recombination is again observed.

The dropoff in CF_2 concentration at times greater than 20 ms could be due to a few different effects. It is possible that the HFPO concentration is being depleted, so that the production rate of CF_2 is slowing down. For HFPO chemistries in pulsed plasmas, Labelle *et al.* have observed that HFPO decomposition actually decreases for longer on times.[20] This suggests that, in the later parts of the plasma on cycle, the rate of reaction (2) decreases. Labelle *et al.* attributed this change to reaction (2) approaching equilibrium. Most studies of HFPO cracking see reaction (2) going to completion,[33] although some evidence of a reversible reaction exists.[34] However, if the cause was an approach to equilibrium, the CF_2 concentration should monotonically approach equilibrium, rather than passing through a maximum. A more likely explanation is a change in the electron energy distribution function that reduces the rate constant of reaction (2) relative to that of reaction (7). To be consistent with Labelle *et al.*'s results, the change must be primarily in reaction (2).

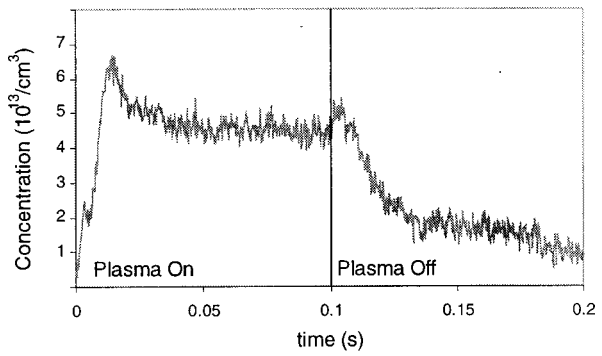

FIG. 6. CF_2 transient for a 100/400 HFPO plasma. The substrate temperature is 20 °C and the wall 60 °C. The chemistry observed here is considerably more complex than in the TFE case, since there are two independent production mechanisms and a consumption mechanism observed in the on time. The off time behavior is similar to that of TFE.

The off time decay is examined for longer off times as shown in Fig. 7. This demonstrates that the decay is again fit well by a second order decay plus a flow term. {Eq. (13) with $[I]=0$}. Again, a first order decay mechanism does not give a good fit of the data, which is consistent with a low gas phase fluorine concentration. The fit parameter for this fit is 3.48×10^{-13} cm^3/s, which is again higher than what is presented in the literature. This probably represents a significant contribution of recombination on the chamber walls. At a higher wall and wafer temperature, a lower recombination coefficient is expected.

IV. CONCLUSIONS

Quantitative time resolved measurements of CF_2 have been measured in pulsed HFPO and TFE plasmas. The on time CF_2 kinetics can be modeled by first order creation and by first and second order destruction mechanisms in the TFE plasma. An initial off time production mechanism has been observed, and this has been related to the observation in other work on surface CF_2 production. An additional background absorption has been observed in the same region as CF_2. The source of this absorption is not clear.

The HFPO plasma behavior is much more complex. Three regimes are observed in the on time, with two independent production mechanisms, and then a reduction in CF_2 concentration. The first regime is believed to be related to decomposition of the feedstock gas. Changes in electron density and temperature appear to cause a reduction in HFPO dissociation rates at longer on times. The off time behavior of HFPO is similar to that observed for TFE, with an initial net production in the off time, followed by consumption by self recombination.

ACKNOWLEDGMENT

The authors would like to thank the DuPont Zyron Gases group for support of this project.

APPENDIX (ESTIMATION OF L_{eff})

The effective length of absorption of the UV signal will depend on the concentration of CF_2 in the reactor:

$$L_{\text{eff}}=\frac{1}{n_{\text{center}}}\int_0^L n(x)dx, \tag{A1}$$

where n_{center} is the concentration in the center of the plasma, and x is along the direction of the UV beam and runs a total length of L. In our system, the plasma is confined to the middle 10 cm of the reactor. The reactor diameter is 20 cm, and viewports add an additional 10 cm to the path of the UV beam. The concentration will thus be divided into three regions:

$$L_{\text{eff}}=2\int_0^{r_0}\tilde{n}_{\text{plasma}}dr+2\int_{r_0}^{R}\tilde{n}_{\text{annular}}dr+2\int_R^{L/2}\tilde{n}_{\text{viewport}}dr, \tag{A2}$$

where $\tilde{n}=n/n_{\text{center}}$. We will assume here that the concentration is approximately uniform in the plasma, so $\tilde{n}_{\text{plasma}}=1$. The rest of the Appendix deals with derivation of the concentration profiles in the annular and viewport regions.

The concentration in the annular region between the electrodes and the chamber wall can be estimated by using the time independent, one-dimensional transport equation:

$$-\frac{D}{r}\frac{d}{dr}\left(r\frac{dn}{dr}\right)+\frac{1}{r}\frac{d}{dr}(rv_rn)=-k_9n^2-\frac{v_z}{d}n, \tag{A3}$$

where the first term represents diffusive transport, the second radial transport, the third is homogeneous recombination, and the last term represents convective flow out of the path of the UV light. These quantities can be made dimensionless by introducing dimensionless variables, $\tilde{v}=v/v_r(r_0)$ and $\eta=r/R$, where r_0 is the radius of the plasma and R is the radius to the chamber wall. The equation then becomes

$$-\frac{1}{Pe}\frac{1}{\eta}\frac{d}{d\eta}\left(\eta\frac{d\tilde{n}}{d\eta}\right)+\frac{1}{\eta}\frac{d}{d\eta}(\eta\tilde{v}_r\tilde{n})=-Da\tilde{n}^2-\frac{\tilde{v}_zR}{d}\tilde{n}, \tag{A4}$$

where the Peclet number, Pe, is given by $v_r(r_0)R/D$ and the Damköhler number, Da, is given by $k_9n_0R/v_r(r_0)$.

The Peclet number represents the relative importance of convective to diffusive transport. Under the conditions here, $v_r(r_0)$ is 476 cm/s, R is 10 cm, and D is about 43 cm^2/s.[35] Thus we find a Peclet number of 111, indicating that convective transport dominates diffusive transport, and that the first term can be neglected. The Damköhler number represents the relative importance of homogeneous reaction to convective transport. Using $10^{14}/\text{cm}^3$ for n_0 and the regressed value of $\sim 1\times 10^{-13}$ cm^3/s for k_9, we find that the Damköhler number is 0.22. So convective transport occurs on a faster scale than reaction, but the difference is less significant than the ratio to diffusive transport. The final dimensionless term represents relative transport in the z direction relative to the r direction. This should be of order 1 based on the two-dimensional continuity equation:

$$\frac{1}{R\eta}\frac{\partial}{\partial\eta}(\rho\eta\tilde{v}_r)+\frac{\partial}{\partial z}(\rho\tilde{v}_z)=0. \tag{A5}$$

If we assume that density variations are small relative to velocity changes (justified by dimensional analysis of the Navier–Stokes equations with the ideal gas law describing the density–pressure relationship), we find

$$\frac{1}{\eta}\frac{\partial}{\partial\eta}(\eta\tilde{v}_r)=-R\frac{\partial\tilde{v}_z}{\partial z}\approx-\frac{R\tilde{v}_z}{d}. \tag{A6}$$

By putting Eq. (A6) into Eq. (A4), one can see that this term will cancel the convective removal term in Eq. (A4). It is now necessary to determine the radial velocity term. To get an approximate solution, we will assume that v_z is independent of the radial position (which will not be consistent with the Navier–Stokes equations, but makes an analytical approximation possible). The boundary condition is given by no radial flow at the wall. This equation is then solved by

$$\tilde{v}_r=\frac{\tilde{v}_zR}{2d}\left(\eta-\frac{1}{\eta}\right). \tag{A7}$$

The value of $\tilde{v}_z$ can be obtained by solving for $r=r_0$:

$$\tilde{v}_z=-\frac{2d}{R}\frac{\eta_0}{1-\eta_0^2}. \tag{A8}$$

The CF_2 transport equation, Eq. (A4), can now be reduced to

$$\tilde{v}_r\frac{d\tilde{n}}{d\eta}=-Da\tilde{n}^2, \tag{A9}$$

with a boundary condition of $\tilde{n}=1$ at η_0, which has the solution

$$\tilde{n}=\left[1-\frac{Da}{2}\frac{\eta_0}{1-\eta_0^2}\ln\left(\frac{\eta^2-1}{\eta_0^2-1}\right)\right]^{-1}. \tag{A10}$$

For the value of Da observed here, this represents a fairly weak dependence of concentration on the radius. Using this equation in Eq. (A2), we find that the annular region will contribute an effective length of 9.4 cm.

In the viewport, flow will be stagnant and the region is described best by Cartesian, not cylindrical, coordinates. The governing equation for mass transport will thus involve only reaction and diffusion:

$$\frac{d^2\tilde{n}}{d\xi^2}=Da_2\tilde{n}^2, \tag{A11}$$

where $\xi=x/l$, where l is the length of the viewport, and Da_2 is the Damköhler number based on diffusion in the viewport, and is given by $k_9n_0L^2/D$. Da_2 equals 0.58 based on the parameters here.

At the entrance to the viewport, the concentration can be found by matching to the concentration in the annular region. Equation (A10) goes to zero at the wall because it is derived assuming that transport is solely convective. This equation does not apply inside the transport boundary layer, where diffusion is the dominant transport mechanism. This boundary layer will begin where the Peclet number is near 1, about 8 mm from the wall (or at $\eta=0.92$). At this point, Eq. (A10) gives $\tilde{n}=0.895$. This will be approximately equal to the concentration at the viewport entrance. The boundary conditions will then given by

$$\tilde{n}(0)\approx 0.89,\qquad \left.\frac{d\tilde{n}}{d\xi}\right|_{\xi=1}=\frac{lk_sn_0}{D}\tilde{n}^2, \tag{A12}$$

where k_s is the recombination coefficient on the surface. k_s can be estimated based on the change in recombination with a colder surface wall. We see an apparent rise in homogeneous recombination of $\sim 2\times 10^{-13}\,\mathrm{cm}^3/\mathrm{s}$. This can be converted into surface reactivity by multiplying by the volume to area ratio, or $R/2$.

A closed form solution of these equations cannot be obtained, however a numerical solution was determined by numerical integration and iteration of boundary conditions, giving a contribution of 6.8 cm to the overall path length. This will be somewhat higher for the case of the heated walls, because the boundary condition approaches zero.

Summing the values estimated from Eqs. (A10)–(A12) and the assumed $\tilde{n}_{\mathrm{plasma}}$, we then get the effective length from Eq. (A12) to be 26.2 cm.

[1] J.-P. Booth, Plasma Sources Sci. Technol. **8**, 249 (1999).
[2] G. S. Oehrlein, M. F. Doemling, B. E. E. Kastenmeier, P. J. Matsuo, N. R. Rueger, M. Schaepkens, and T. E. F. M. Standaert, IBM J. Res. Dev. **43**, 1 (1999).
[3] J. A. Theil, J. Vac. Sci. Technol. B **17**, 2397 (1999).
[4] W. Schwarzenbach, G. Cunge, and J. P. Booth, J. Appl. Phys. **85**, 7562 (1999).
[5] S. J. Limb, D. J. Edell, E. F. Gleason, and K. K. Gleason, J. Appl. Polym. Sci. **67**, 1489 (1998).
[6] L. W. Anderson, A. N. Goyette, and J. E. Lawyer, Adv. At., Mol., Opt. Phys. **43**, 295 (2000).
[7] J. A. O'Neill and J. Singh, J. Appl. Phys. **76**, 5967 (1994).
[8] J. A. O'Neill and J. Singh, J. Appl. Phys. **77**, 497 (1995).
[9] J.-P. Booth, G. Cunge, F. Neuilly, and N. Sadeghi, Plasma Sources Sci. Technol. **7**, 423 (1998).
[10] M. Haverlag, W. W. Stoffels, E. Stoffels, J. H. W. G. d. Boer, G. M. W. Kroesen, and F. J. de Hoog, Plasma Sources Sci. Technol. **4**, 260 (1995).
[11] M. Haverlag, W. W. Stoffels, E. Stoffels, G. M. W. Kroesen, and F. J. de Hoog, J. Vac. Sci. Technol. A **14**, 384 (1996).
[12] J. Wormhoudt, J. Vac. Sci. Technol. A **8**, 1722 (1990).
[13] J. P. Booth, G. Cunge, P. Chabert, and N. Sadeghi, J. Appl. Phys. **85**, 3097 (1999).
[14] G. Cunge and J. P. Booth, J. Appl. Phys. **85**, 3952 (1999).
[15] C. Suzuki, K. Sasaki, and K. Kadota, J. Vac. Sci. Technol. A **16**, 2222 (1998).
[16] C. Suzuki, K. Sasaki, and K. Kadota, J. Appl. Phys. **82**, 5321 (1997).
[17] S. G. Hansen, G. Luckman, and S. D. Colson, Appl. Phys. Lett. **53**, 1588 (1988).
[18] C. Suzuki, K. Sasaki, and K. Kadota, Jpn. J. Appl. Phys., Part 1 **37**, 5763 (1998).
[19] R. d'Agostino, F. Cramarossa, and S. D. Benectidis, Plasma Chem. Plasma Process. **2**, 213 (1982).
[20] C. B. Labelle, S. M. Karecki, R. L. Reif, and K. K. Gleason, J. Vac. Sci. Technol. A **17**, 3419 (1999).
[21] S. Sharpe, B. Hartnett, H. S. Sethi, and D. S. Sethi, J. Photochem. **38**, 1 (1987).
[22] D. S. King, P. K. Schenck, and J. C. Stephenson, J. Mol. Spectrosc. **78**, 1 (1979).
[23] R. Holland and J. L. Lyman, J. Quant. Spectrosc. Radiat. Transf. **38**, 79 (1987).
[24] A. Kono, M. Haverlag, G. M. W. Kroesen, and F. J. de Hoog, J. Appl. Phys. **70**, 2939 (1991).
[25] Y. Hikosaka and H. Sugai, Jpn. J. Appl. Phys., Part 1 **32**, 3040 (1993).
[26] D. C. Gray, Ph.D. thesis, Massachusetts Institute of Technology, 1992.
[27] H. Sugai, K. Nakamura, Y. Hikosaka, and M. Nakamura, J. Vac. Sci. Technol. A **13**, 887 (1995).
[28] M. Inayoshi, M. Ito, M. Hori, T. Goto, and M. Hiramatsu, J. Vac. Sci. Technol. A **16**, 233 (1998).
[29] W. J. R. Tyerman, Trans. Faraday Soc. **65**, 1188 (1969).
[30] K. Sasaki, Y. Kawai, C. Suzuki, and K. Kadota, J. Appl. Phys. **82**, 5938 (1997).
[31] N. E. Capps, N. M. Mackie, and E. R. Fisher, J. Appl. Phys. **84**, 4736 (1998).
[32] B. A. Cruden, K. Chu, K. K. Gleason, and H. H. Sawin, J. Electrochem. Soc. **146**, 4590 (1999).
[33] R. C. Kennedy and J. B. Levy, J. Fluorine Chem. **7**, 101 (1976).
[34] W. Mahler and P. R. Resnick, J. Fluorine Chem. **3**, 451 (1973/4).
[35] S. J. Limb, Ph.D. thesis, Massachusetts Institute of Technology, 1997.